Design of On-Body Epidermal Antenna on AMC Substrate for UHF RFID in Healthcare

Giovanni Andrea Casula, *Senior Member, IEEE*, Francesco Lestini, *Graduate Student Member, IEEE*, Francesco Paolo Chietera, *Member, IEEE*, Giacomo Muntoni, Cecilia Occhiuzzi, *Senior Member, IEEE*, Luca Catarinucci, *Senior Member, IEEE*, Riccardo Colella, *Senior Member, IEEE*, Giorgio Montisci, *Senior Member, IEEE*, and Gaetano Marrocco, *Senior Member, IEEE*

***Abstract*— This article presents a compact AMC structure used as a shielding element for a generic wearable RFID tag at UHF frequencies for on-body applications, with an overall footprint limited to an area of only 0.03 λ_0^2 (41.4 × 82.8 mm). Thanks to the isolation provided by the AMC planar structure, the tag antenna gain and reading range are increased by about one order of magnitude in comparison with the case of a conventional tag attached to the human body. The designed antenna is platform tolerant, with very good robustness and isolation with respect to the human body, exhibiting a high reliability. The AMC structure is implemented on a thin, flexible, and biocompatible high permittivity silicon-doped dielectric substrate, with apertures both in the substrate and in the ground plane to allow skin transpiration. Therefore, the presented device can be effectively used also as an epidermal antenna, allowing the "on-skin" sampling of the most typical health parameters. The presented configuration has been designed using CST Studio Suite. A prototype has been fabricated and fully characterized, and measured results are in very good agreement with simulations.**

***Index Terms*— Artificial magnetic conductor (AMC), epidermal antenna, healthcare, RFID antenna.**

I. Introduction

THE recent advance in pervasive remote assistance and healthcare digitalization is favoring the diffusion and development of biomedical services and systems, able to empower patients to have a central role in their personal care and health diagnostic and monitoring [1], [2]. The growth of these services and applications calls for the study of new challenges and alternative approaches for the design of wearable, implantable, and biocompatible devices. The latter can rely on electromagnetic fields for gathering and analyzing several categories of data (physiological, emotional, behavioral, environmental), aiming to improve citizens' well-being and health [2].

In this framework, wearable electronics represent an emerging research trend that combines multidisciplinary backgrounds such as classic electronics and electromagnetics, material science, communication, and mechanics [3], [4], [5], [6]. Wearable electronics and sensors can be easily deployed and/or integrated over users' garments, enabling a hugeness of new applications for human health and wellness. The most effective way to collect the data acquired by wearable sensors is using wireless technology, and the well-assessed passive radio frequency identification (RFID) technology is certainly one of the best candidates [7], also allowing easy interfacing with the increasingly widespread the Internet of Things [8]. As a matter of fact, RFID technology is based on communication through electromagnetic backscattering. It requires just a small battery-less IC transponder, which is fully compatible with wearable, flexible, and thin devices ensuring a reading range up to 10 m in the UHF frequency band [7]. Furthermore, most recent RFID ICs integrate also some physical sensing capabilities (e.g., temperature and humidity [9]) or, complementary, analog ports, and A/D converters to straightforwardly interface external sensors. As a consequence, RFID platforms can retrieve some important data and information about the state of the human body by exploiting the simple interaction between the tag and the skin [10], with no need for dedicated and complex electronics that should be integrated into the wearable device otherwise [11].

The main drawback of this solution is due to the high losses of the platform on which the wearable device is attached, the human body, which strongly degrades the performance of the RFID tag antenna, decreasing the efficiency and the reading range, detuning the antenna resonant frequency, and deteriorating the radiated electromagnetic far-field. All these effects are strictly related to the antenna size, layout, and operating frequency. Moreover, the geometrical and electromagnetic parameters of the human body, on which the antenna is attached, may also differ based on the antenna location (e.g., head, chest, leg, arm) even on the same person [12], [13], [14], [15], [16]. On-body platform tolerant devices are then a must. Such devices should be designed to seamlessly, unobtrusively, and comfortably adhere to the textured and soft surfaces, typical of the human body, and are required to provide a low density of surface conductors. Therefore,

Manuscript received 4 December 2023; revised 6 March 2024; accepted 24 March 2024. Date of publication 4 April 2024; date of current version 7 May 2024. *(Corresponding author: Giovanni Andrea Casula.)*

Giovanni Andrea Casula, Giacomo Muntoni, and Giorgio Montisci are with the Dipartimento di Ingegneria Elettrica ed Elettronica, Università degli Studi di Cagliari, 09123 Cagliari, Italy (e-mail: andrea.casula@unica.it; giacomo.muntoni@unica.it; giorgio.montisci@unica.it).

Francesco Lestini, Cecilia Occhiuzzi, and Gaetano Marrocco are with the Pervasive Electromagnetics Laboratory, University of Rome "Tor Vergata," 00133 Rome, Italy (e-mail: f.lestini97@gmail.com; cecilia.occhiuzzi@uniroma2.it; gaetano.marrocco@uniroma2.it).

Francesco Paolo Chietera, Luca Catarinucci, and Riccardo Colella are with the Department of Innovation Engineering, University of Salento, 73100 Lecce, Italy (e-mail: francescopaolo.chietera@unisalento.it; luca.catarinucci@unisalento.it; riccardo.colella@unisalento.it).

Color versions of one or more figures in this article are available at https://doi.org/10.1109/TAP.2024.3383214.

Digital Object Identifier 10.1109/TAP.2024.3383214

preferably, they should be designed using narrow conductor traces and thin dielectric substrates [3], [4], [5], [6]. The optimal substrate structure must be flexible, with a relatively high dielectric constant and low losses (for example a suitable doped silicone substrate, which can allow an adequate size reduction, obtaining a compact and comfortable epidermal device) [11], [17]. The radiating part of the device, which will ensure the correct transfer of data and information, requires an adequate UHF-RFID tag antenna that should be fabricated through the same technology of the sensor device.

An on-body antenna typically consists of aperture antennas, wherein an arbitrary shaped slot is etched into a metal patch [18], [19], planar inverted-F antennas [13], [15], [20], [21], or patch antennas. The antenna–body coupling effect can be reduced by using appropriate insulating substrates [22], or suitably enlarging the antenna's ground plane [21], [23], allowing effective shielding between the antenna and the human body. This ensures better insulation, but robustness is achieved at the expense of a larger antenna, leading to an obtrusive and uncomfortable device, especially at the UHF band, although a proper shape of the ground plane can be chosen with a reduced impact on the antenna extent [13], [15], [16], [24]. Moreover, such wearable antennas (both aperture, patch, and PIFAs) require thick dielectric substrates and/or suitable air gaps to properly work in proximity to the body tissues.

An alternative, and most effective, solution to obtain a more performing device is found in artificial magnetic conductors (AMCs) [25], [26], [27]. This solution can be exploited by the designer to preserve the RFID tag antenna radiation characteristic, thanks to the capability of an AMC to isolate an antenna from the surrounding environment. Moreover, the use of the AMC as a tag support will enhance the RFID antenna gain, which is strongly reduced by the coupling with the human body when the tag is directly attached to it [28].

A large number of papers present different approaches to improve on-body antenna performance using AMC supporting structures [27], [29], [30], [31], [32], [33], [34], [35], [36], [37], [38], [39], [40], [41], [42], [43], [44], [45], [46], with single [27], [29], [30], [33], [34], [35], [36], [37], [38], [39], [40], [41], [42], [43], [44], [45], [46] and dual-band behavior [31], [32]. Only a few of them are designed in the lowest part of UHF frequency band, for RFID applications [29], [30], and this is mainly due to the difficulties of designing a compact and effective AMC structure at these frequencies.

AMC supporting structures play a pivotal role as effective shielding elements, thereby enhancing the performance of on-body antennas. This inherent characteristic of AMCs, which constitutes their primary advantage, can be effectively leveraged for a generic antenna attached to the AMC, provided that the antenna size is smaller than the AMC structure. The generic antenna supported by the AMC can take the form of a wire antenna or rely on a planar design. The optimal performance may require a gap between the antenna and the AMC. This gap can be easily implemented using suitable materials such as foams or supporting dielectric structures. The increase in antenna gain, achieved through the isolation offered by the planar AMC structure, depends on the layout of the supported antenna. For example, in the case of a planar inverted-F antenna (see [42], [46]) with an existing ground plane, the gain improvement due to the AMC is limited to a few decibels. Conversely, for antennas without inherent isolation, such as our generic tag or the structures reported in [45] (a printed monopole) or in [34] (a printed Yagi-Uda antenna), the gain improvement can exceed 10 dB. This highlights the crucial role of supporting AMC in achieving a satisfactory realized gain under typical operating conditions. Additionally, the resulting structure demonstrates platform tolerance, exhibiting good isolation and robustness with respect to the working environment.

In this work, we present the design, characterization, and validation of a relatively small AMC structure used as a shielding element for a wearable RFID tag at UHF frequencies. A generic RFID tag antenna has been attached to the miniaturized AMC, suitably designed to limit the overall footprint of the radiating antenna to an area of only 0.03 λ_0^2 (41.4×82.8 mm), a very small size if compared to the state of the art for an AMC-based antenna (see Table I). This compact radiating device is designed to operate within the RFID UHF frequency band, at the central frequency of 900 MHz. The performance of the tag in two specific operating conditions has been investigated and compared, i.e., when directly attached to the human body and when placed upon a tailored AMC structure, which shields it from the wearer. A substantial increase of the tag antenna gain (and, consequently, of the reading range) of about one order of magnitude has been achieved, thanks to the isolation provided by the AMC planar structure, which can be considered a significant improvement in the platform-tolerant device performance. The gain increase (14 dB) is considerable, also if compared to the typical increment achieved by similar proposed devices [27], [29], [30], [31], [32], [33], [34], [35], [36], [37], [38], [39], [40], [41], [42], [43], [44], [45], [46] (see Table I) and allows the wearable antenna to reach a satisfying reading range in typical operating conditions.

The designed antenna is considered platform tolerant, presenting very good isolation and robustness with respect to the human body, a satisfying reading range, and high reliability.

In addition, we adopted very thin dielectric substrates for both the AMC and RFID tag, purposely realizing and shaping the AMC substrate to exhibit an adequately high dielectric constant, low losses, flexibility, biocompatibility, and breathability (thanks to holes in the substrate). For the same reason, also the AMC ground plane is properly shaped, proposing a thin and flexible on-body antenna. As a consequence, our RFID tag can be used also as an epidermal antenna, allowing the "on-skin" sampling of typical health parameters, such as surface/body temperature, pH, humidity, skin impedance, deformations, fluid exchanges at the skin interface and electrophysiological potentials. This tag can operate without interfering with the local metabolism of the skin, since its breathable substrate does not perturb the skin's local temperature and transpiration, resulting in a minimal impact on local sweating and heat exchanges. In Table I, we compared our device also with two epidermal antennas proposed in recent literature [47], [48], which show

TABLE I
COMPARISON WITH THE STATE-OF-THE-ART

Ref.	f_{res}(MHz)	ε_r	H_z (mm)	Area (λ_0^2)	Gain on body (dBi)	Gain on body with AMC (dBi)	Gain increment (dBi)	Epidermal	Flexible	On AMC
[27]	2450	2.5	1.55 (0.0127 λ_0)	0.288	-	-	3.7	No	Yes	Yes
[29]	868	10.2	2 (0.0058 λ_0)	0.061	-	-	2.9	No	Yes	Yes
[30]	915	4.4	6.4 (0.0195 λ_0)	0.422	-2.44	5.01	7.45	No	No	Yes
[31]	2450 5800	3	13.16 (0.107 λ_0)	0.037	2.44 6.17	-	-	No	Yes	Yes
[32]	3500 5000	3.55	7 (0.082 λ_0)	0.611	-	-	-	No	Yes	Yes
[33]	2400	1.7	2.4 (0.0192 λ_0)	0.135	-	-	7.8	No	No	Yes
[34]	2400	2.8	-	1.17	-7.09	7.9	14.99	No	No	Yes
[35]	2450	2.2	6.57 (0.054 λ_0)	0.172	-	6.88	-	No	Yes	Yes
[36]	2450	2.9	3.5 (0.0286 λ_0)	0.382	5.14	-	11.54	No	Yes	Yes
[37]	2450	4.4	3.3 (0.027 λ_0)	0.193	-7	3	10	No	No	Yes
[38]	5450	2.7	2 (0.036 λ_0)	1	-	7.63	1.2	No	No	Yes
[39]	2450	1.8	7.6 (0.062 λ_0)	0.627	4.01	7.15	3.14	No	Yes	Yes
[40]	5800	2.3	3 (0.058 λ_0)	3.74	-3.83	-0.55	3.28	No	Yes	Yes
[41]	2450	3	5.12 (0.042 λ_0)	1	-1.69	8.4	10.09	No	No	Yes
[42]	2000	10.2	4.75 (0.032 λ_0)	0.058	2.8	4.6	1.8	No	No	Yes
[43]	2450	3.31	9.5 (0.064 λ_0)	0.11	-	0.12	-	No	Yes	Yes
[44]	2000	1.44	6 (0.04 λ_0)	0.89	0	3.38	3.38	No	Yes	Yes
[45]	2400	3	4 (0.032 λ_0)	0.167	-8	5.7	13.7	No	Yes	Yes
[46]	5500	1.2	4 (0.073 λ_0)	0.395	5.2	6.7	1.5	No	Yes	Yes
[47]	868	4.18	0.089 (0.00026 λ_0)	8.8/103	-18.1	-	-	Yes	Yes	No
[48]	868	2.8	1 (0.0029 λ_0)	0.0283	-15.3	-	-	Yes	Yes	No
This Work	900	6.24	2.405 (0.0072 λ_0)	0.03	-22	-8	14	Yes	Yes	Yes

unsatisfying performance in terms of realized gain, since they work attached to the skin, without any countermeasure with respect to the interaction with the human body.

II. AMC DESIGN

An AMC is a particular electromagnetic bandgap (EBG) structure [49], [50] designed to emulate the properties of an AMC within the designated frequency range. EBG structures, generally characterized by their periodic or sometimes non-periodic nature, exert control over the propagation of electromagnetic waves across a defined frequency band, accommodating all incident angles and polarization states. These periodic structures exhibit resonance at specific frequencies, manifesting filtering characteristics that find applications at microwave frequencies, offering advantages such as compactness and high gain [49], [50].

The AMC operation is based on the resonance of the cavity between the ground plane and the periodic elements. Therefore, AMCs are narrowband devices. The shape of the periodic elements ranges from simple (patches, dipoles) to complex geometries [51] and, due to the resonant behavior of the AMC device, the size of the unit cell must be close to half a wavelength.

By employing an AMC, it is possible to place a planar electric source close (or attached) to the meta-surface without degrading its performance, since the AMC has only a negligible effect on its radiating properties. This could be very important in wearable applications, wherein the AMC features can be exploited to obtain high robustness and isolation between the antenna and its platform (the human body). Moreover, this solution allows a significant increase in the gain of a planar electric source when compared with its gain when it radiates in free space or even when attached to the human body (which represents a significantly worse situation).

AMC structures have been widely used in recent years for several applications: as ground planes for antennas [52], as resonant structures [45], for improving the transmission of waves from nearby wearable antennas [53], for antenna

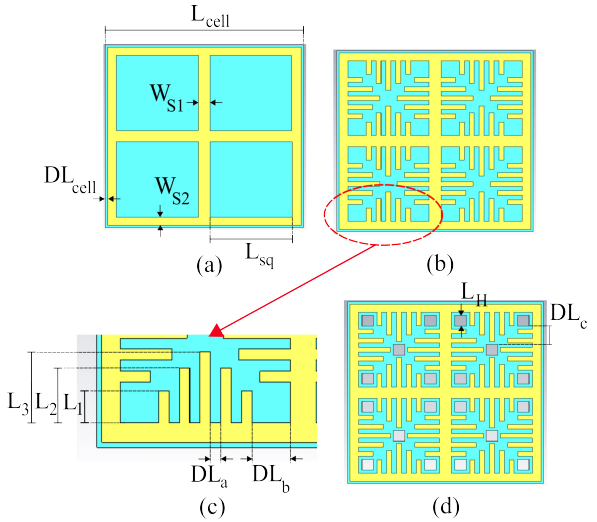

Fig. 1. (a) Top view of the conventional AMC unit cell. $L_{cell} = 41.4$ mm; $W_{S1} = 2.55$ mm; $W_{S2} = 1.84$ mm; $DL_{cell} = 0.5$ mm; $L_{sq} = 17$ mm. (b) Top view of the modified AMC unit cell. (c) Zoomed-in view of the region with the comb-like arms. $DL_a = 1$ mm; $DL_b = 3.85$ mm; $L_1 = 3$ mm; $L_2 = 5.2$ mm; $L_3 = 6.7$ mm. The width of each metallic arm is 1 mm. (d) Top view of the modified AMC unit cell with rectangular holes in substrate and ground plane. $DL_c = 4.15$ mm; $L_H = 2.45$ mm.

impedance matching [54], for antenna detection [55], for radiating element shielding and SAR reduction [27], and as tunable devices [56].

Unfortunately, AMC unit cells can be cumbersome, mainly in the lower part of the UHF band, wherein even half a wavelength can be an unpractical size in several applications. Therefore, a challenging aspect of AMC design is to minimize the size of the periodic unit cell. In [57] and [58] the AMC device has been miniaturized using convoluted elements and space-filling curves as unit cells, but these solutions reduce the operating bandwidth.

A better solution to obtain the AMC reduction has been achieved in this work by modifying a conventional symmetric square unit cell inspired by the classical bidimensional cell, namely the *"Jerusalem cross"* [59], [60], whose circuital model can be considered equivalent to a parallel *LC* circuit. In such EBG structures, the equivalent capacitance *C* is mainly related to the gap between two adjacent elementary EBG cells, whereas the equivalent inductance *L* is due to the thin microstrip lines connecting the cells.

We started our design with a conventional symmetric square unit cell [depicted in Fig. 1(a)], which we modified through the incorporation of enhanced features in the form of comb-like arms on each side of the metallic squares [illustrated in Fig. 1(b) and (c)]. These arms play a crucial role in extending the path of the current flowing through the structure. Each of these comb-like arms introduces an additional inductance to the cell equivalent parallel *LC* circuit, determined by the length of the arms. Furthermore, the presence of these arms introduces an additional capacitance, which is influenced by the spacing between these arms. The cumulative effect of these modifications results in the new AMC cell resonating at a lower frequency compared to its conventional counterpart. The overall capacitance of the cell is subject to further fine-tuning through adjustments in the spacing between neighboring cells [intercell distance DL_{cell}, as depicted in Fig. 1(a)]. The cell size and its design parameters (intercell spacing DL_{cell}, lengths of comb-like arms L_1, L_2, L_3 and their spacing DL_a, DL_b) have been carefully selected to ensure resonance at 900 MHz, within the RFID UHF frequency band.

A. Permittivity-Tailored AMC Supporting Substrate

As previously mentioned, a significant challenge in designing and implementing an AMC structure for UHF frequencies lies in achieving a compact size. Properly designing the periodic structure is a crucial factor in obtaining this outcome. Equally important is the precise design and fabrication of a high-permittivity substrate. Moreover, the substrate dielectric constant should be carefully tailored to match the very strict design constraints: indeed, even slight variations in the substrate properties could lead to a not-effectively-working device because of the narrowband behavior of the AMC structure.

To properly realize a substrate with the above features, we have mixed a silicone rubber matrix with a highly ferroelectric ceramic filler to produce a nanocomposite material having the desired properties [61]. Silicone rubber is chosen because it is a biocompatible, nontoxic, and non-irritant material. It typically consists of two components mixed in a 1:1 ratio to initiate the polymerization process, causing the silicone to solidify. During this initial phase, the silicone remains processable, allowing for the addition of filler into the silicone matrix and the pouring of the composite material into the mold before polymerization starts. The mixing process can be performed manually or with specialized mixers to minimize the introduction of air into the composite. The presence of microbubbles of air is the main factor leading to degradation in dielectric properties and can occur during both mixing and casting procedure. The ceramic filler utilized was Barium Titanate ($BaTiO_3$), known for its distinctive electrical properties, including a high dielectric constant and piezoelectric behavior. However, its dielectric constant significantly relies on its lattice structure, which can be hexagonal, tetragonal, or cubic, determined by the production process and sintering temperature [62]. Additionally, $BaTiO_3$ exhibits a Curie Temperature of approximately 120 °C. Beyond this point, it undergoes a lattice transformation to the cubic form, resulting in a reduction of the dielectric constant. Consequently, this value can vary widely, ranging from tens to thousands. For the above reason, the adopted Barium Titanate has been previously characterized in [63] and resulted in a dielectric constant of 250, which remains valid as long as the mixing process is performed at room temperature and, in general, the threshold temperature of 120 °C is never exceeded. To estimate the effective dielectric constant of the final substrate, the Lichtenecker's model [64] was employed, which is defined by the following formula:

$$ln(\varepsilon_{eff}) = f_1\ ln(\varepsilon_1) + f_2\ ln(\varepsilon_2) \tag{1}$$

where ε_{eff} is the dielectric constant of the final composite material, ε_1 and ε_2 are the dielectric constant of both matrix and filler (3.25 and 250, respectively), and f_1, f_2 are the volume percentage of the materials.

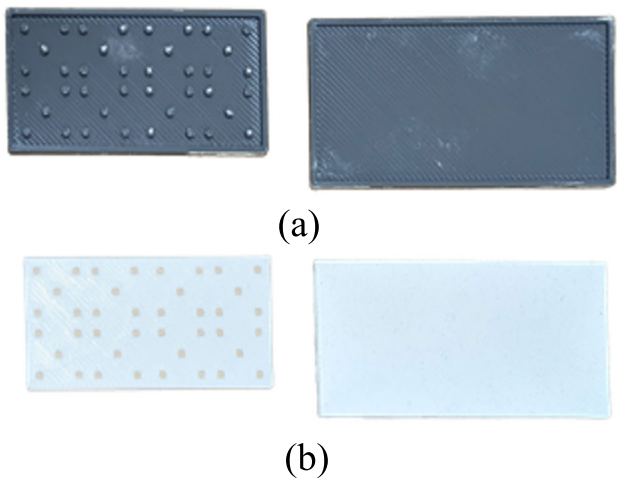

Fig. 2. (a) Some of the 3-D-printed molds of the realized substrates: the custom one on the left and the bulk one on the right. (b) Silicone-based substrates after the casting process.

Our goal was to realize a substrate of the AMC having a value of ε_{eff} between 6.2 and 6.3 and this result was achieved by utilizing, according to (1), a filler percentage of around 16%. To allow for a correct measurement of dielectric constant and loss tangent, in the same realization process, a bulk dielectric of $10 \times 5 \times 0.15$ cm^3 along with the desired customized dielectric substrate has been created. The electromagnetic characterization of the bulk substrate at 866 MHz, performed using the well-known T-Resonator method [65], resulted in a measured dielectric constant of 6.24 and a loss tangent of 0.0135. Specifically, as for substrate shaping, an additive manufacturing technology called fused filament fabrication (FFF) has been used for 3-D-printing the container (mold) in which the silicone-based composite was cast. Molds and substrates are shown in Fig. 2.

The fabricated doped silicone substrate is flexible and has a relatively high dielectric constant with relatively low losses, hence it allows an adequate size reduction, obtaining a compact and comfortable wearable antenna.

B. AMC Unit Cell Numerical Results

The final AMC design has a unit cell with periodicity $D = 41.4$ mm ($0.12\ \lambda_0$ at 900 MHz) and a total thickness of 1.57 mm ($0.0047\ \lambda_0$ at 900 MHz). The conventional AMC cell with the same geometry will resonate at 1.15 GHz, therefore, the comb-like arms allow a size reduction of 28%.

Both the amplitude and phase of the reflection coefficient of the AMC structure for an incident plane wave are reported in Fig. 3 for different values of the substrate height h_s. This is a key parameter for the AMC, which will influence both the resonant frequency and the operating frequency band (defined as the frequency range where the phase varies from $-90°$ to $+90°$ [49], [50], [66]).

As reported in the frequency response of the designed unit cell, depicted in Fig. 3, increasing the AMC substrate thickness h_s leads to an increase in the operating bandwidth and a reduction of the resonant frequency. Moreover, when the thickness h_s is lower than 3 mm, the AMC exhibits

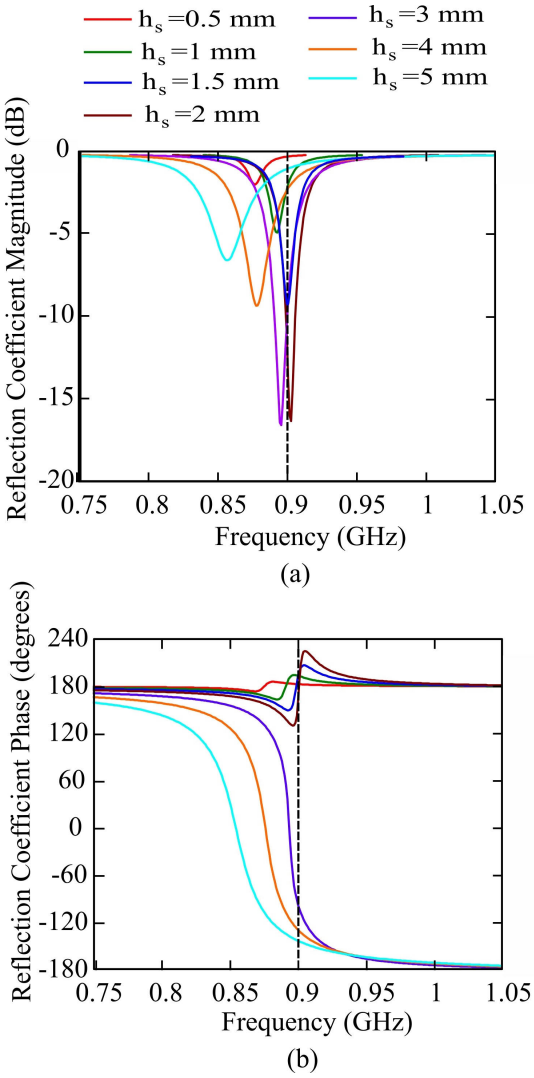

Fig. 3. Frequency response of the proposed AMC cell. (a) Reflection coefficient magnitude and (b) phase.

only a partial inversion of the phase. However, since epidermal antennas should guarantee unobtrusive and comfortable operation, a thickness above 3 mm is not acceptable, as the substrate height needs to be as small as possible. Therefore, it is crucial to reduce the thickness as much as possible. Thus, to address this constraint, we opted to fix the value of h_s at 1.5 mm. Despite the fact that such reduced thickness allows only a partial inversion of the AMC phase, as apparent also from Figs. 3(b) and 4, this is adequate to ensure satisfactory performance for the designed on-body epidermal antenna (AMC + RFID tag), when the antenna is attached to the human body. This is evidenced by the results presented in the next section, which showcase the performance of the designed structure.

In order to ensure adequate perspiration of the skin, both the AMC substrate and ground plane should be drilled, making a sufficient number of holes. The cell of Fig. 1(b) is therefore modified by inserting five small rectangular openings in each of the four quadrants, as shown in Fig. 1(d), giving the structure a band-aid-like layout.

The frequency response of this unit cell is shown in Fig. 4, where it is compared with the cell without holes, showing only

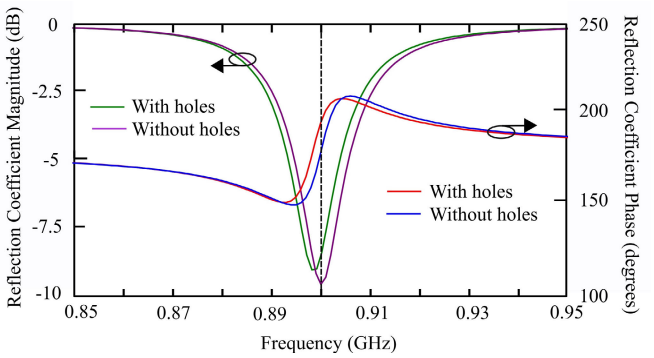

Fig. 4. Frequency response of the meandered AMC screen with and without openings.

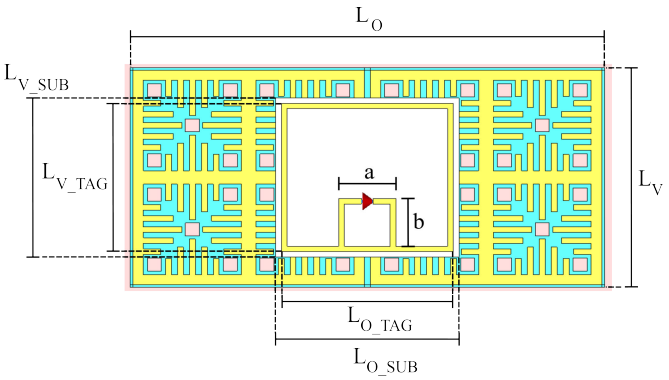

Fig. 5. Designed wearable antenna. $L_O = 82.8$ mm; $L_V = 41.4$ mm; $L_{O\_SUB} = 32$ mm; $L_{V\_SUB} = 30$ mm; $L_{O\_TAG} = 30$ mm; $L_{V\_TAG} = 28$ mm; $a = 10$ mm; $b = 9$ mm.

a negligible frequency shift, which does not affect the AMC performance.

III. Antenna Numerical Results and On-Body Performance

The AMC designed in the previous section is used as a shielding element for an on-body RFID tag operating within the RFID UHF frequency band, at the central frequency of 900 MHz. A loop antenna attached to the miniaturized AMC structure (see Fig. 5) has been selected. It consists of a standard rectangular metallic loop on a Rogers RT/Duroid 5880 substrate [67]. The Duroid has a thickness of $h_{sub} = 0.8$ mm and dimensions $L_{O\_SUB} = 32$ mm, $L_{V\_SUB} = 30$ mm, with dielectric permittivity $\varepsilon_r = 2.2$ and $\tan\delta = 0.0009$. The tag metallic traces are made of copper with a thickness of 0.035 mm and a width of $w_{tag} = 1$ mm. The tag is connected to the Magnus S3 integrated circuit (IC) by Axzon with impedance $Z_{chip} = 4\text{-j}93\ \Omega$ (corresponding to the *RC* model indicated in the datasheet [68], with $R_p = 2073\ \Omega$ and $C_p = 1.9$ pF, computed at 900 MHz) and chip sensitivity (i.e., the minimum power required to turn-on the IC) $P_{IC} = -13.3$ dBm$p_{\text{IC}} = -13.3$ dBm, by means of a T-match for impedance matching purposes [69]. The finite AMC structure placed underneath the tag antenna is composed of an array of 2×1-unit cells (see Fig. 5), which represents the smallest possible size for a finite AMC, hence the proposed on-body/epidermal antenna has a very compact size of $41.4 \times 82.8 \times 2.405$ mm^3 ($2.2 \times 10^{-4}\lambda_0^3$ at 900 MHz).

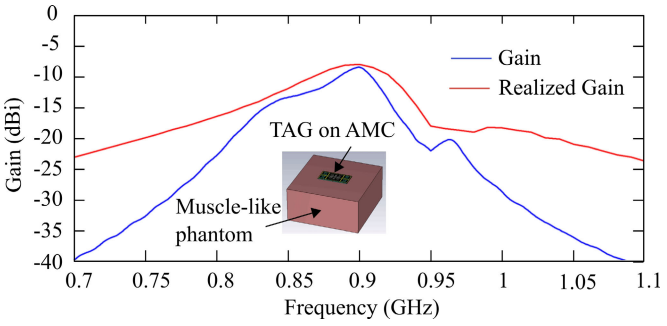

Fig. 6. Simulated gain and realized gain of the proposed wearable antenna.

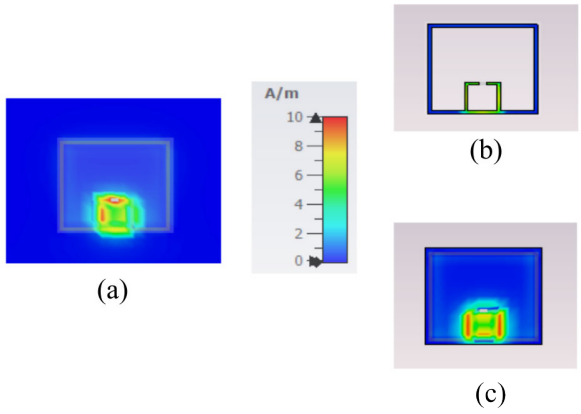

Fig. 7. Magnetic field magnitude on (a) phantom, (b) tag's metallic loop, and (c) tag's dielectric substrate when the tag is directly attached to the phantom.

The rectangular tag optimal geometrical parameters $L_{O\_TAG} = 30$ mm and $L_{V\_TAG} = 28$ mm $L_{O\_TAG} = 30$ mm were chosen based on the result of a parametric analysis oriented to the optimization of the far-field gain G. In a similar fashion, the T-match dimensions $a = 10$ mm and $b = 9$ mm were chosen in order to match the tag impedance with that of the microchip, so that also the tag realized gain G_τ (i.e., the antenna gain G scaled by the impedance mismatch with the microchip [69]) was optimized. Both gain and realized gain are shown in Fig. 6.

In order to highlight the increase in the performance of the tag due to the insertion of the AMC shielding structure, two operating conditions have been investigated and compared: 1) the tag directly attached to the human body and 2) the tag placed upon the tailored AMC structure.

We used a single-layer equivalent model as a numerical phantom to analyze the body-antenna coupling effect on the antenna performance. It consists of a 100 mm-thick material with an area of 200×200 mm^2 (see Fig. 6) and with electrical parameters $\varepsilon_r = 55$ and $\sigma = 0.94$ S/m at 900 MHz [70].

In Figs. 7–12, the simulated magnetic field, electric field, and surface current distributions are shown for the operating conditions 1) and 2), respectively.

The presented results clearly highlight that the AMC structure acts as a shielding layer between the antenna and the human body, and the stacked structure (tag on AMC) shows significantly smaller peak values for both electric fields (an order of magnitude lower), magnetic field, and surface current (four times lower), ensuring very good isolation and robustness with respect to the human body. This behavior is confirmed

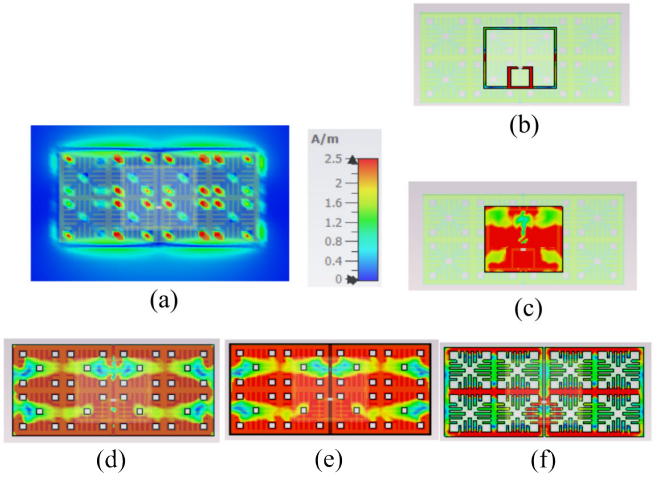

Fig. 8. Magnetic field magnitude on (a) phantom, (b) tag's metallic loop, (c) tag's dielectric substrate, (d) AMC drilled ground plane, (e) AMC dielectric substrate, (f) AMC metallic trace when the tag is placed upon the tailored AMC structure.

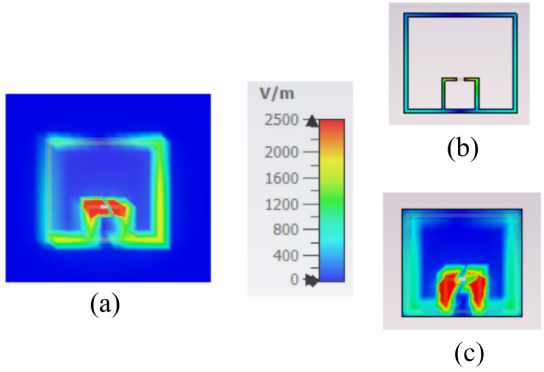

Fig. 9. Electric field magnitude on (a) phantom, (b) tag's metallic loop, and (c) tag's dielectric substrate when the tag is directly attached to the phantom.

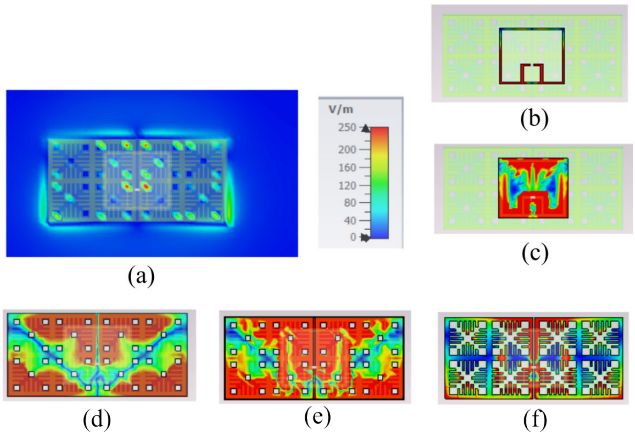

Fig. 10. Electric field magnitude on (a) phantom, (b) tag's metallic loop, (c) tag's dielectric substrate, (d) AMC drilled ground plane, (e) AMC dielectric substrate, and (f) AMC metallic trace when the tag is placed upon the tailored AMC structure.

by the far-field pattern in Fig. 13, with the tag placed upon the AMC structure having a smaller cross polar component if compared with the tag directly attached to the phantom (10 dB lower in the peak values, and more than 35 dB lower in the

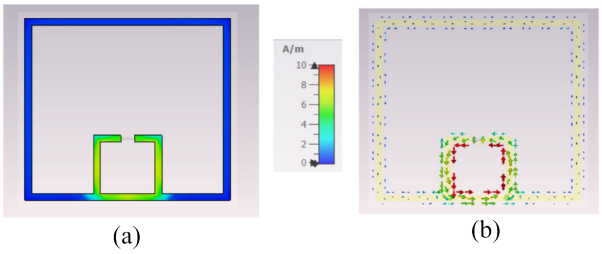

Fig. 11. Surface current (a) magnitude and (b) vector on the tag's metallic loop when the tag is directly attached to the phantom.

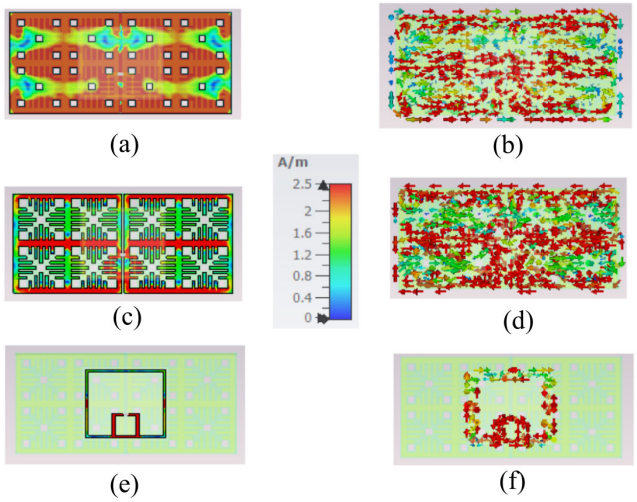

Fig. 12. Surface current (a) magnitude and (b) vector on the AMC drilled ground plane, (c) magnitude and (d) vector on the AMC metallic trace, and (e) magnitude and (f) vector on the tag's metallic loop when the tag is placed upon the tailored AMC structure.

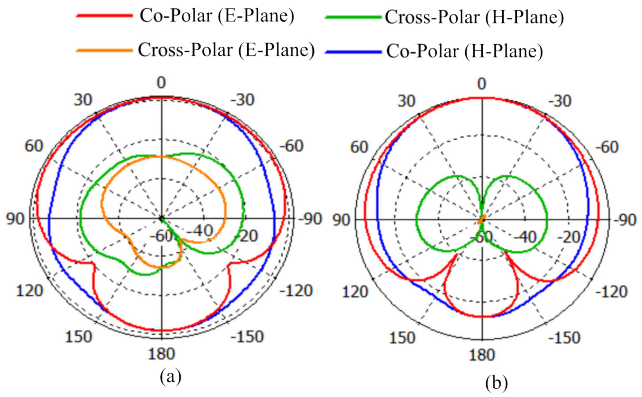

Fig. 13. Far-field pattern (a) when the tag is directly attached to the phantom and (b) when the tag is placed upon the tailored AMC structure.

broadside direction), with a front-to-back ratio greater than 18 dB.

Finally, Fig. 14 shows the increase of the tag antenna gain when it is attached to the AMC structure and placed on the phantom, with respect to the gain of the tag directly attached to the phantom without the support of the AMC. A considerable increment of 14 dB is achieved, which corresponds to a significant improvement in the performance of the proposed on-body/epidermal device, allowing it to reach a very good reading range.

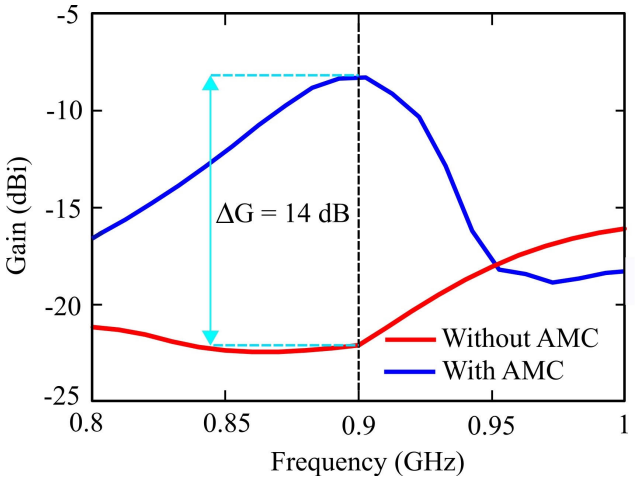

Fig. 14. Simulated Gain for the tag attached to the AMC structure and placed on the phantom, and for the tag directly attached to the phantom without the support of the AMC structure.

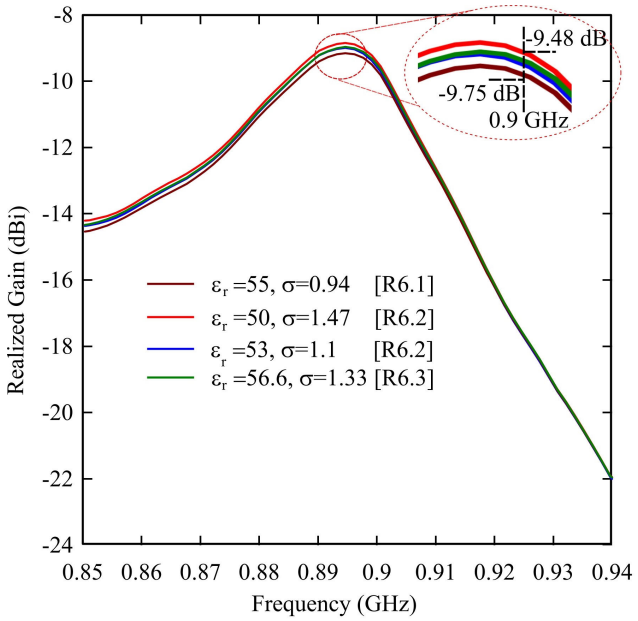

Fig. 15. Comparison between simulated realized gains for the proposed tag attached to the flat muscle-like phantom depicted in Fig. 6 with different electric parameters.

The improvement in antenna performance due to the insertion of the AMC is closely linked to the specific design of the supported antenna. The inherent shielding feature of AMCs can be efficiently employed for any generic antenna attached to the AMC, as long as the antenna is smaller than the AMC structure. Looking at the state-of-the-art structures reported in Table I, it is evident that the AMC functions effectively and independently of the supported antenna. The key difference lies in the increase in gain and enhancement in isolation, both of which depend on the particular layout of the antenna under consideration.

IV. Sensitivity Analysis and Bending Assessment

To assess the sensitivity and robustness of the proposed on-body epidermal antenna, a comprehensive analysis was conducted to evaluate its performance under various conditions, encompassing different phantom models and bending scenarios. The literature provides varying dielectric constant values for muscle tissue, with discrepancies attributed to factors such as measurement inaccuracies, subject age, or the specific muscle type under consideration. Leveraging literature-derived data for muscle tissues at 900 MHz, we applied parameters sourced from [70], [71], and [72] to simulate the muscle-like phantom. In Fig. 15, we compared the simulated realized gains for the proposed tag attached to the flat muscle-like phantom depicted in Fig. 6 with the electric parameters given by [70] ($\varepsilon_r = 55$ and $\sigma = 0.94$ S/m), [71] ($\varepsilon_r = 50$ and $\sigma = 1.47$ S/m for a temperature of T = 15 °C, $\varepsilon_r = 53$ and $\sigma = 1.1$ S/m for T = 30 °C), and [72] ($\varepsilon_r = 56.6$ and $\sigma = 1.33$ S/m). Despite the differences in dielectric constant and conductivity among the considered phantoms, the presented results demonstrate minimal impact on the antenna performance. At the design frequency of 900 MHz, the maximum difference among the four curves is only 0.27 dB, showing the low sensitivity of the proposed tag.

Additionally, we also assessed the structure's robustness under bending conditions using a multilayered cylinder simulating a human leg. This model incorporates skin, fat, muscle, and bone layers (refer to Fig. 16 for a detailed illustration of this multilayer model and for the electrical parameters assigned to each layer at 900 MHz). The bone diameter (D_b)

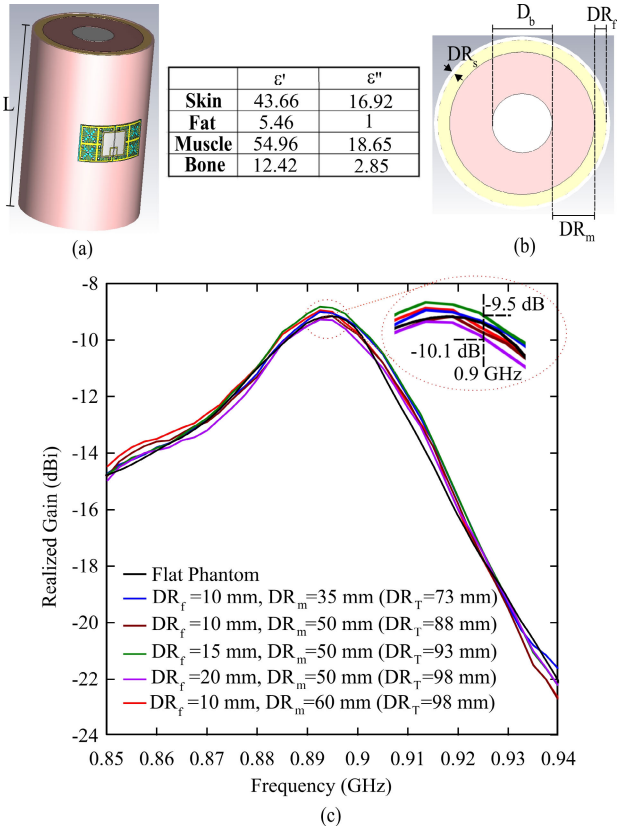

Fig. 16. (a) Three-dimensional view of the multilayer model of the human leg with attached the bent tag ($L = 200$ mm). (b) Top view of the multilayer model of the human leg. $DR_S = 3$ mm, $D_b = 50$ mm. (c) Comparison between simulated realized gains for the proposed tag attached to the multilayer leg model for different thicknesses of muscle and fat layers, and hence for different bending diameters DR_T (as explicitly indicated in the curves labels).

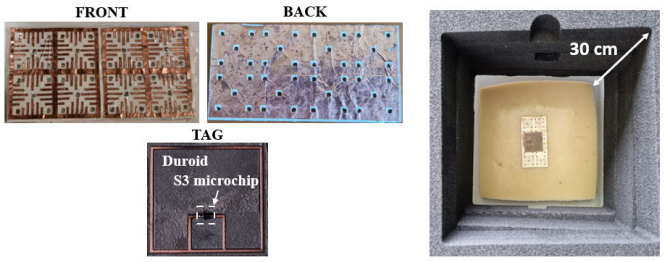

(a) (b)

Fig. 17. (a) Front view and back view of the prototype of the AMC structure of the designed wearable antenna, and front view of the Tag. (b) Antenna attached to the muscle-equivalent gelatinous phantom inserted into the rotating platform.

was set to 50 mm, and the skin layer thickness (DR_S) to 3 mm. By varying the thicknesses of the muscle and fat layers, and consequently adjusting the overall leg diameter, we explored different antenna bending diameters (DR_T) ranging from 73 to 98 mm. This parametric exploration allowed us to evaluate the antenna sensitivity also in the context of a multilayer cylindrical phantom model. Despite the substantial variations in layer thickness, the antenna exhibited remarkable stability in performance. At the design frequency of 900 MHz, the maximum difference among the six curves was only 0.6 dB, with a difference lower than 0.4 dB compared to the flat muscle-like phantom in Fig. 6. This resilience across diverse scenarios can be attributed to the high isolation provided by the supporting AMC structure. It highlights the platform tolerance of our structure, showing its low sensitivity to changes in phantom properties and structure, and its robustness when subjected to bending.

V. On-Body/Epidermal Antenna Experimental Verification

A prototype of the proposed on-body/epidermal antenna has been realized and fully characterized. The drilled AMC array and ground plane [see Fig. 17(a)] were etched from an adhesive copper sheet and then attached to the substrate. The RFID tag [see Fig. 17(a)] was realized by etching the copper from the Duroid substrate, whereas the microchip was soldered with the help of a bench soldering iron. Moreover, the resulting structure was entirely covered with a thin film of Tegaderm [73] to stabilize the prototype and ensure that all its components were joined together.

Figs. 17(b) and 18 show the measurement setup. The realized on-body antenna was placed above a hydrogel-composed muscle-like phantom (by AET, [74]) with size 200 × 200 × 70 mm, relative permittivity $\varepsilon_r = 54.5$ $\varepsilon_r = 54.5$ and conductivity $\sigma = 0.6$ S/m$\sigma = 0.6$ S/m, that was refurbished by water 48 h before use and placed on a rotating platform [see Fig. 15(b)]. A circularly polarized antenna (patch with broadside gain $G_R = 7.5$ dBic) was placed 30 cm above the prototype and connected to the TagFormance UHF Pro station for realized gain and radiation pattern measurements purposes (see Fig. 18). Finally, the antenna was also attached to the chest of a volunteer by means of another Tegaderm adhesive substrate in order to perform measurements also in a real case scenario (see Fig. 18).

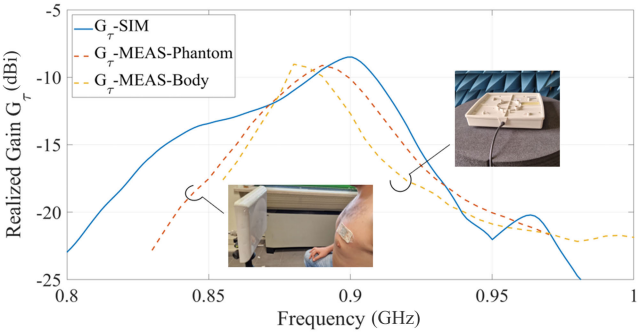

Fig. 18. Comparison between simulated and measured realized gains. Measures have been performed both with the tag antenna attached to a muscle-like phantom and to a volunteer, according to the setups shown in the figure insets.

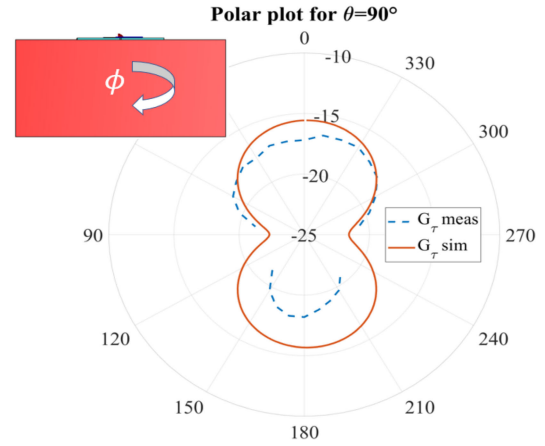

(a)

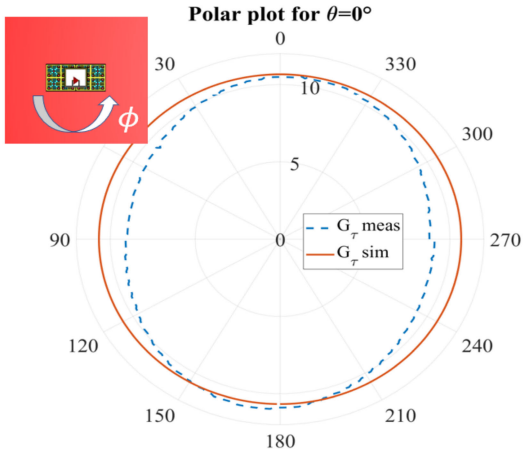

(b)

Fig. 19. Simulated and measured far-field pattern in the two main cuts ($\theta = 0°$ and $\theta = 90°$). The measures have been performed by means of a rotating platform.

The comparison between simulated and measured realized gains is shown in Fig. 18. The peak values of the measured realized gains are almost equal, whereas a slight difference with the simulated one is observed. Moreover, there is also a small frequency shift between all of them. These differences could be ascribed to uncertainties in prototype realization

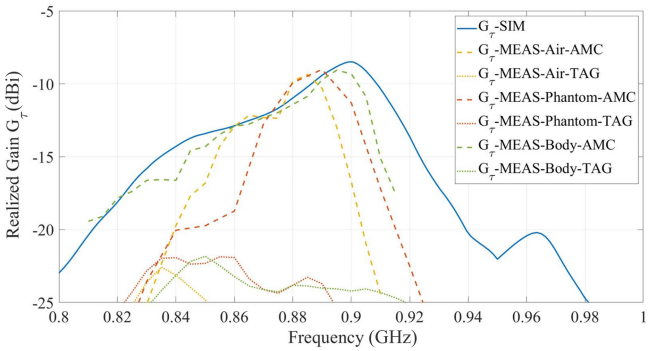

Fig. 20. Measured realized gain of the tag + AMC and of the sole tag in three different operative conditions, in air, on the phantom, and on the human body.

and dielectric properties of both the muscle-like phantom and volunteer skin. Despite this, measurements and simulations fit very well. Finally, radiation pattern measurements of the tag for $\theta = 0°\theta = 0°$ and $\theta = 90°$ (see Fig. 19) were performed as well. Also, in this case, there is a good agreement between simulations and measurements.

To further verify the proposed AMC decoupling capabilities, a new set of measurements was performed (see Fig. 20). The measurements show the realized gain of the tag + AMC and of the sole tag in three conditions, i.e., air, human body, and human phantom. While the tag + AMC offers the same realized gain regardless of the object to which it is attached (and well in line with simulations), the sole tag is sensibly affected by the operative conditions, suffering detuning, impedance mismatching, and efficiency worsening (the realized gain is sensibly lower and shifted in frequency).

By considering the FRIIS formula, the realized gain can be related to the expected maximum activation distance d [7]

$$d = \frac{\lambda}{4\pi}\sqrt{\frac{EIRPG\tau\chi}{Pic}}. \quad (2)$$

With λ the wavelength at 900 MHz, EIRP is the effective isotropic power radiated by the reader, χ the polarization mismatch between reader and tag, and Pic the power sensitivity of the IC. In the case of EIRP = 3.2 W (the maximum power level allowed by ETSI regulations), $Pic = -13.3$ dBm and $\chi = 1$, the expected maximum activation distance $d = 3$ m.

VI. Conclusion

In this work, a novel on-body/epidermal antenna on a miniaturized AMC structure has been designed, exploiting the AMC to improve the performance of healthcare RFID applications. The AMC miniaturization has been achieved by suitably meandering a conventional unit cell and using a house-made high-permittivity and low-losses thin and flexible silicone-doped dielectric substrate.

The antenna works within the RFID UHF frequencies around 900 MHz, and its overall footprint is limited to an area of only 0.03 λ_0^2 (41.4 × 82.8 mm). The isolation provided by the AMC planar structure allows to increase in the tag antenna gain and reading range of about one order of magnitude in comparison with the case of the conventional tag (without AMC) attached to the human body.

The proposed device is platform tolerant, with high reliability, and is implemented on a very thin, flexible, and biocompatible substrate, with an adequate number of holes both in the AMC substrate and ground plane to allow skin transpiration. Such features ensure that the designed structure can be effectively used also as an epidermal antenna, allowing the "on-skin" sampling of the most typical health parameters like body temperature, skin impedance, and electrophysiological potentials.

Acknowledgment

The authors would like to thank Simone Nappi and Carolina Miozzi for their useful advice.

References

[1] Z. N. Chen, *Antennas for Portable Devices*, 1st ed. Chichester, U.K.: Wiley, 2007.
[2] D. H. Werner and Z. H. Jiang, *Electromagnetics of Body Area Networks: Antennas, Propagation and RF Systems*, 1st ed. Hoboken, NJ, USA: Wiley, 2016.
[3] J. J. Rutherford, "Wearable technology," *IEEE Eng. Med. Biol. Mag.*, vol. 29, no. 3, pp. 19–24, May 2010.
[4] Z. Wang, Z. Yang, and T. Dong, "A review of wearable technologies for elderly care that can accurately track indoor position, recognize physical activities and monitor vital signs in real time," *Sensors*, vol. 17, no. 2, p. 341, Feb. 2017.
[5] Y.-M. de-la-Fuente-Robles, A.-J. Ricoy-Cano, A.-P. Albín-Rodríguez, J. L. López-Ruiz, and M. Espinilla-Estévez, "Past, present and future of research on wearable technologies for healthcare: A bibliometric analysis using scopus," *Sensors*, vol. 22, no. 22, p. 8599, Nov. 2022.
[6] J. McCann and D. Bryson, *Smart Clothes and Wearable Technology* (The Textile Institute Book Series), 2nd ed. Amsterdam, The Netherlands: Elsevier, 2022.
[7] D. M. Dobkin, *The RF in RFID: UHF RFID in Practice*. Amsterdam, The Netherlands: Elsevier, 2008.
[8] F. Costa, S. Genovesi, M. Borgese, A. Michel, F. A. Dicandia, and G. Manara, "A review of RFID sensors, the new frontier of Internet of Things," *Sensors*, vol. 21, no. 9, p. 3138, Apr. 2021.
[9] F. Camera, C. Miozzi, F. Amato, C. Occhiuzzi, and G. Marrocco, "Experimental assessment of wireless monitoring of axilla temperature by means of epidermal battery-less RFID sensors," *IEEE Sensors Lett.*, vol. 4, no. 11, pp. 1–4, Nov. 2020, doi: 10.1109/LSENS.2020.3036486.
[10] C. Occhiuzzi and G. Marrocco, "Precision and accuracy in UHF-RFID power measurements for passive sensing," *IEEE Sensors J.*, vol. 16, no. 9, pp. 3091–3098, May 2016, doi: 10.1109/JSEN.2016.2526678.
[11] C. Occhiuzzi, S. Caizzone, and G. Marrocco, "Passive UHF RFID antennas for sensing applications: Principles, methods, and classifications," *IEEE Antennas Propag. Mag.*, vol. 55, no. 6, pp. 14–34, Dec. 2013.
[12] G. A. Casula, G. Montisci, and H. Rogier, "A wearable textile RFID tag based on an eighth-mode substrate integrated waveguide cavity," *IEEE Access*, vol. 8, pp. 11116–11123, 2020.
[13] A. Michel et al., "Design considerations on the placement of a wearable UHF-RFID PIFA on a compact ground plane," *IEEE Trans. Antennas Propag.*, vol. 66, no. 6, pp. 3142–3147, Jun. 2018.
[14] G. A. Casula, G. Montisci, G. Valente, and G. Gatto, "A robust printed antenna for UHF wearable applications," *IEEE Trans. Antennas Propag.*, vol. 66, no. 8, pp. 4337–4342, Aug. 2018.
[15] G. A. Casula, A. Michel, P. Nepa, G. Montisci, and G. Mazzarella, "Robustness of wearable UHF-band PIFAs to human-body proximity," *IEEE Trans. Antennas Propag.*, vol. 64, no. 5, pp. 2050–2055, May 2016.
[16] G. A. Casula, A. Michel, G. Montisci, P. Nepa, and G. Valente, "Energy-based considerations for ungrounded wearable UHF antenna design," *IEEE Sensors J.*, vol. 17, no. 3, pp. 687–694, Feb. 2017.
[17] A. Ajovalasit et al., "Development and characterization of xyloglucan-poly(vinyl alcohol) hydrogel membrane for wireless smart wound dressings," *Eur. Polym. J.*, vol. 106, pp. 214–222, Sep. 2018.
[18] G. Marrocco, "RFID antennas for the UHF remote monitoring of human subjects," *IEEE Trans. Antennas Propag.*, vol. 55, no. 6, pp. 1862–1870, Jun. 2007.

[19] C. Occhiuzzi, S. Cippitelli, and G. Marrocco, "Modeling, design and experimentation of wearable RFID sensor tag," *IEEE Trans. Antennas Propag.*, vol. 58, no. 8, pp. 2490–2498, Aug. 2010.

[20] M.-H. Lin and C.-W. Chiu, "Human-body effects on the design of card-type UHF RFID tag antennas," in *Proc. IEEE Int. Symp. Antennas Propag. (APSURSI)*, Jul. 2011, pp. 521–524.

[21] C.-H. Lin, K. Saito, M. Takahashi, and K. Ito, "A compact planar inverted-F antenna for 2.45 GHz on-body communications," *IEEE Trans. Antennas Propag.*, vol. 60, no. 9, pp. 4422–4426, Sep. 2012.

[22] F. Merli, B. Fuchs, J. R. Mosig, and A. K. Skrivervik, "The effect of insulating layers on the performance of implanted antennas," *IEEE Trans. Antennas Propag.*, vol. AP-59, no. 1, pp. 21–31, Jan. 2011.

[23] S. Agneessens, S. Lemey, T. Vervust, and H. Rogier, "Wearable, small, and robust: The circular quarter-mode textile antenna," *IEEE Antennas Wireless Propag. Lett.*, vol. 14, pp. 1482–1485, 2015.

[24] G. Casula and G. Montisci, "A design rule to reduce the human body effect on wearable PIFA antennas," *Electronics*, vol. 8, no. 2, p. 244, Feb. 2019.

[25] S. Zhu and R. Langley, "Dual-band wearable textile antenna on an EBG substrate," *IEEE Trans. Antennas Propag.*, vol. 57, no. 4, pp. 926–935, Apr. 2009.

[26] S. Kim, Y. Ren, H. Lee, A. Rida, S. Nikolaou, and M. M. Tentzeris, "Monopole antenna with inkjet-printed EBG array on paper substrate for wearable applications," *IEEE Antennas Wireless Propag. Lett.*, vol. 11, pp. 663–666, 2012.

[27] H. R. Raad, A. I. Abbosh, H. M. Al-Rizzo, and D. G. Rucker, "Flexible and compact AMC based antenna for telemedicine applications," *IEEE Trans. Antennas Propag.*, vol. 61, no. 2, pp. 524–531, Feb. 2013.

[28] S. Amendola, C. Occhiuzzi, and G. Marrocco, "More than wearable: Epidermal antennas for tracking and sensing," in *Electromagnetics of Body Area Networks: Antennas Propagation and RF Systems*. Hoboken, NJ, USA: Wiley, 2016.

[29] R. C. Hadarig, M. E. de Cos, and F. Las-Heras, "UHF dipole-AMC combination for RFID applications," *IEEE Antennas Wireless Propag. Lett.*, vol. 12, pp. 1041–1044, 2013.

[30] J. H. Hong, C.-W. Chiu, and H.-C. Wang, "design of circularly polarized tag antenna with artificial magnetic conductor for on-body applications," *Prog. Electromagn. Res. C*, vol. 81, pp. 89–99, 2018.

[31] M. A. Shahzad et al., "An artificial magnetic conductor-backed compact wearable antenna for smart watch IoT applications," *Electronics*, vol. 10, no. 23, p. 2908, Nov. 2021.

[32] J. Zhang, J. Meng, W. Li, S. Yan, and G. A. E. Vandenbosch, "A wearable button antenna sensor for dual-mode wireless information and power transfer," *Sensors*, vol. 21, no. 17, p. 5678, Aug. 2021.

[33] A. Y. I. Ashyap et al., "Compact and low-profile textile EBG-based antenna for wearable medical applications," *IEEE Antennas Wireless Propag. Lett.*, vol. 16, pp. 2550–2553, 2017.

[34] B. S. Abirami and E. F. Sundarsingh, "EBG-backed flexible printed Yagi–Uda antenna for on-body communication," *IEEE Trans. Antennas Propag.*, vol. 65, no. 7, pp. 3762–3765, Jul. 2017.

[35] M. A. B. Abbasi, S. S. Nikolaou, M. A. Antoniades, M. N. Stevanovic, and P. Vryonides, "Compact EBG-backed planar monopole for BAN wearable applications," *IEEE Trans. Antennas Propag.*, vol. 65, no. 2, pp. 453–463, Feb. 2017.

[36] M. E. Atrash, O. F. Abdalgalil, I. S. Mahmoud, M. A. Abdalla, and S. R. Zahran, "Wearable high gain low SAR antenna loaded with backed all-textile EBG for WBAN applications," *IET Microw., Antennas Propag.*, vol. 14, no. 8, pp. 791–799, Jul. 2020.

[37] D. Wen, Y. Hao, M. O. Munoz, H. Wang, and H. Zhou, "A compact and low-profile MIMO antenna using a miniature circular high-impedance surface for wearable applications," *IEEE Trans. Antennas Propag.*, vol. 66, no. 1, pp. 96–104, Jan. 2018.

[38] G. Gao, R.-F. Zhang, W.-F. Geng, H.-J. Meng, and B. Hu, "Characteristic mode analysis of a nonuniform metasurface antenna for wearable applications," *IEEE Antennas Wireless Propag. Lett.*, vol. 19, no. 8, pp. 1355–1359, Aug. 2020.

[39] R. Pei et al., "Wearable EBG-backed belt antenna for smart on-body applications," *IEEE Trans. Ind. Informat.*, vol. 16, no. 11, pp. 7177–7189, Nov. 2020.

[40] J. Tak, Y. Hong, and J. Choi, "Textile antenna with EBG structure for body surface wave enhancement," *Electron. Lett.*, vol. 51, no. 15, pp. 1131–1132, Jul. 2015.

[41] A. Alemaryeen and S. Noghanian, "Crumpling effects and specific absorption rates of flexible AMC integrated antennas," *IET Microw., Antennas Propag.*, vol. 12, no. 4, pp. 627–635, Mar. 2018.

[42] S. I. Kwak, D.-U. Sim, J. H. Kwon, and Y. J. Yoon, "Design of PIFA with metamaterials for body-SAR reduction in wearable applications," *IEEE Trans. Electromagn. Compat.*, vol. 59, no. 1, pp. 297–300, Feb. 2017.

[43] K. Agarwal, Y. Guo, and B. Salam, "Wearable AMC backed near-endfire antenna for on-body communications on latex substrate," *IEEE Trans. Compon., Packag., Manuf. Technol.*, vol. 6, no. 3, pp. 346–358, Mar. 2016.

[44] E. F. N. M. Hussin, P. J. Soh, M. F. Jamlos, H. Lago, A. A. Al-Hadi, and M. H. F. Rahiman, "A wideband textile antenna with a ring-slotted AMC plane," *Appl. Phys. A, Solids Surf.*, vol. 123, no. 1, p. 46, Jan. 2017.

[45] Z. Jiang, D. E. Brocker, P. E. Sieber, and D. H. Werner, "A compact, low-profile metasurface-enabled antenna for wearable medical body-area network devices," *IEEE Trans. Antennas Propag.*, vol. 62, no. 8, pp. 4021–4030, Aug. 2014.

[46] G.-P. Gao, C. Yang, B. Hu, R.-F. Zhang, and S.-F. Wang, "A wearable PIFA with an all-textile metasurface for 5 GHz WBAN applications," *IEEE Antennas Wireless Propag. Lett.*, vol. 18, no. 2, pp. 288–292, Feb. 2019.

[47] R. B. V. B. Simorangkir et al., "Screen printed epidermal antenna for IoT health monitoring," in *Proc. IEEE Asia–Pacific Microw. Conf. (APMC)*, Nov. 2021, pp. 395–397.

[48] R. B. V. B. Simorangkir et al., "Transparent epidermal antenna for unobtrusive human-centric Internet of Things applications," *IEEE Internet Things J.*, vol. 11, no. 1, pp. 1164–1174, Jan. 2024.

[49] M. S. Alam, N. Misran, B. Yatim, and M. T. Islam, "Development of electromagnetic band gap structures in the perspective of microstrip antenna design," *Int. J. Antennas Propag.*, vol. 2013, pp. 1–22, Jun. 2013.

[50] S. Sarkar and B. Gupta, "Artificial magnetic conductor with self-complementary unit cells having very high angular stability," *Electron. Lett.*, vol. 56, no. 14, pp. 704–706, Jul. 2020.

[51] S. Genovesi, A. Monorchio, R. Mittra, and G. Manara, "A sub-boundary approach for enhanced particle swarm optimization and its application to the design of artificial magnetic conductors," *IEEE Trans. Antennas Propag.*, vol. 55, no. 3, pp. 766–770, Mar. 2007.

[52] S. X. Ta and I. Park, "Dual-band low-profile crossed asymmetric dipole antenna on dual-band AMC surface," *IEEE Antennas Wireless Propag. Lett.*, vol. 13, pp. 587–590, 2014.

[53] K. Kamardin, M. K. Abd Rahim, N. A. Samsuri, M. E. B. Jalil, and I. H. Idris, "Textile artificial magnetic conductor waveguide jacket for on-body transmission enhancement," *Prog. Electromagn. Res. B*, vol. 54, pp. 45–68, 2013.

[54] B. S. Cook and A. Shamim, "Utilizing wideband AMC structures for high-gain inkjet-printed antennas on lossy paper substrate," *IEEE Antennas Wireless Propag. Lett.*, vol. 12, pp. 76–79, 2013.

[55] I. Park and D. Kim, "Artificial magnetic conductor loaded long-range passive RFID tag antenna mountable on metallic objects," *Electron. Lett.*, vol. 50, no. 5, pp. 335–336, Feb. 2014.

[56] F. Costa, A. Monorchio, S. Talarico, and F. M. Valeri, "An active high-impedance surface for low-profile tunable and steerable antennas," *IEEE Antennas Wireless Propag. Lett.*, vol. 7, pp. 676–680, 2008.

[57] J. McVay, N. Engheta, and A. Hoorfar, "High impedance metamaterial surfaces using Hilbert-curve inclusions," *IEEE Microw. Wireless Compon. Lett.*, vol. 14, no. 3, pp. 130–132, Mar. 2004.

[58] B. Sanz-Izquierdo, E. A. Parker, J.-B. Robertson, and J. C. Batchelor, "Singly and dual polarized convoluted frequency selective structures," *IEEE Trans. Antennas Propag.*, vol. 58, no. 3, pp. 690–696, Mar. 2010.

[59] C. R. Simovski, P. de Maagt, and I. V. Melchakova, "High-impedance surfaces having stable resonance with respect to polarization and incidence angle," *IEEE Trans. Antennas Propag.*, vol. 53, no. 3, pp. 908–914, Mar. 2005.

[60] M. Hosseini and M. Hakkak, "Characteristics estimation for Jerusalem cross-based artificial magnetic conductors," *IEEE Antennas Wireless Propag. Lett.*, vol. 7, pp. 58–61, 2008.

[61] S. Koulouridis, G. Kiziltas, Y. Zhou, D. J. Hansford, and J. L. Volakis, "Polymer–ceramic composites for microwave applications: Fabrication and performance assessment," *IEEE Trans. Microw. Theory Techn.*, vol. 54, no. 12, pp. 4202–4208, Dec. 2006, doi: 10.1109/TMTT.2006.885887.

[62] N. H. Yusoff, R. A. M. Osman, M. S. Idris, K. N. D. K. Muhsen, and N. I. M. Nor, "Dielectric and structural analysis of hexagonal and tetragonal phase $BaTiO_3$," in *Proc. AIP Conf.*, Jan. 2020, pp. 1–15, doi: 10.1063/1.5142130.

[63] L. Catarinucci, F. P. Chietera, and R. Colella, "Permittivity-customizable ceramic-doped silicone substrates shaped with 3-D-printed molds to design flexible and conformal antennas," *IEEE Trans. Antennas Propag.*, vol. 68, no. 6, pp. 4967–4972, Jun. 2020.

[64] A. V. Goncharenko, V. Z. Lozovski, and E. F. Venger, "Lichtenecker's equation: Applicability and limitations," *Opt. Commun.*, vol. 174, nos. 1–4, pp. 19–32, Jan. 2000.

[65] R. Colella, F. P. Chietera, F. Montagna, A. Greco, and L. Catarinucci, "Customizing 3D-printing for electromagnetics to design enhanced RFID antennas," *IEEE J. Radio Frequency Identif.*, vol. 4, no. 4, pp. 452–460, Dec. 2020.

[66] S. Trinh-Van et al., "A low-profile high-gain and wideband log-periodic meandered dipole array antenna with a cascaded multi-section artificial magnetic conductor structure," *Sensors*, vol. 19, no. 20, p. 4404, Oct. 2019.

[67] (Mar. 2024). *Rogers Corporation. Rt/Duroid? 5880 Laminates Datasheet*. Rogers Corp. [Online]. Available: https://www.rogerscorp.com/advanced-electronics-solutions/rt-duroid-laminates/rt-duroid-5880-laminates

[68] Axzon. (2021). *RFM3300-E Magnus-S3 M3E Passive Sensor IC*. [Online]. Available: https://axzon.com/rfm3300-e-magnus-s3-m3e-passive-sensor-ic/

[69] G. Marrocco, "The art of UHF RFID antenna design: Impedance-matching and size-reduction techniques," *IEEE Antennas Propag. Mag.*, vol. 50, no. 1, pp. 66–79, Feb. 2008, doi: 10.1109/MAP.2008.4494504.

[70] A. Kiourti and K. S. Nikita, "Miniature scalp-implantable antennas for telemetry in the MICS and ISM bands: Design, safety considerations and link budget analysis," *IEEE Trans. Antennas Propag.*, vol. 60, no. 8, pp. 3568–3575, Aug. 2012.

[71] C. Chou, G. Chen, A. W. Guy, and K. H. Luk, "Formulas for preparing phantom muscle tissue at various radiofrequencies," *Bioelectromagnetics*, vol. 5, no. 4, pp. 435–441, Jan. 1984.

[72] G. Hartsgrove, A. Kraszewski, and A. Surowiec, "Simulated biological materials for electromagnetic radiation absorption studies," *Bioelectromagn., J. Bioelectromagn. Soc., Soc. Phys. Regulation Biol. Med., Eur. Bioelectromagn. Assoc.*, vol. 8, no. 1, pp. 29–36, 1987.

[73] D. R. Seshadri, N. D. Bianco, A. N. Radwan, C. A. Zorman, and K. M. Bogie, "An absorbent, flexible, transparent, and scalable substrate for wound dressings," *IEEE J. Transl. Eng. Health Med.*, vol. 10, pp. 1–9, 2022.

[74] (Mar. 2024). *AET Associates Inc. Human Body Equivalent Phantom*. [Online]. Available: https://www.aetassociates.com/hardware.php?phantom

Giovanni Andrea Casula (Senior Member, IEEE) received the M.S. degree in electronic engineering and the Ph.D. degree in electronic engineering and computer science from the University of Cagliari, Cagliari, Italy, in 2000 and 2004, respectively.

Since December 2017, he has been an Associate Professor of electromagnetic fields at the University of Cagliari, teaching courses in electromagnetics and antenna engineering. He has authored or coauthored about 50 papers in international journals. His current research interests include the analysis and design of waveguide slot arrays, RFID Antennas, wearable antennas, and numerical methods in electromagnetics.

Prof. Casula is an Associate Editor of IEEE TRANSACTIONS ON ANTENNAS AND PROPAGATION, *IET Microwaves, Antennas and Propagation*, MDPI *Electronics*, MDPI *Sensors*, and an Academic Editor of the *International Journal of Antennas and Propagation*.

Francesco Lestini (Graduate Student Member, IEEE) received the B.S. and M.S. degrees (Hons.) in medical engineering from the University of Rome "Tor Vergata," Rome, Italy, in 2019 and 2021, respectively, where he is currently pursuing the Ph.D. degree in computer science, control and geo-information with the Pervasive Electromagnetics Laboratory. Since 2023, he has been a part-time Research and Development Medical Engineer with RADIO6ENSE Srl. His research focuses on RFID-based reconfigurable intelligent surfaces (RIS), to provide them with wireless and low-power reconfigurability. He is also interested in the development of an epidermal RFID grid for distributed skin temperature measurement.

Mr. Lestini is also part of the Cyber4Health observatory, which focuses on raising international awareness about the need for premarket regulations related to the Cyber and Physical security of medical devices. He was a recipient of the Best Paper Award at the seventh edition of the SpliTech Conference in 2022 on Smart and Sustainable Technologies.

Francesco Paolo Chietera (Member, IEEE) received the M.S. degree in communication engineering and the Ph.D. degree from the University of Salento, Lecce, Italy, in 2018 and 2024, respectively.

He is currently engaged as a Researcher within the Electromagnetic Solutions for Hi-Tech (EMTech) Laboratory, Department of Innovation Engineering, University of Salento. He coauthored more than 35 papers on these topics both in international journals and conferences. He is also involved in various financed projects with national and international institutions like the National Institute for Insurance Against Industrial Injuries (INAIL), the National Research Council (CNR), and ERASMUS+. His main research interests include 3D-printing in electromagnetics, with a particular focus on RFID technologies for sensing and traceability, and the IoT-enabling communication technologies in general.

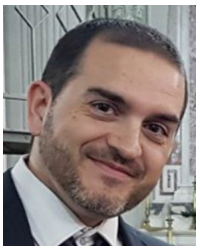

Giacomo Muntoni received the bachelor's degree in electronic engineering, the master's degree in telecommunication engineering, and the Ph.D. degree in electronic engineering and computer science from the University of Cagliari, Cagliari, Italy, in 2010, 2015, and 2019, respectively.

He is currently working as a Technologist with the Applied Electromagnetics Group, University of Cagliari. His research interests include the design and characterization of antennas for biomedical and aerospace applications, microwave-based dielectric characterization of materials, 3-D printing of RF components, and monitoring of the space debris environment in low Earth orbit with the Sardinia Radio Telescope, in collaboration with the Cagliari Astronomical Observatory.

Cecilia Occhiuzzi (Senior Member, IEEE) received the M.Sc. degree in medical engineering and the Ph.D. degree from the University of Rome "Tor Vergata," Rome, Italy, in 2008 and 2011, respectively.

She is currently an Associate Professor with the University of Rome "Tor Vergata," where she teaches electromagnetic fields, biomedical interaction, and instrumentation and techniques for health monitoring and therapy. She is also the Co-Founder and CEO of RADIO6ENSE, a spin-off of the University of Tor Vergata active in RFID solutions for the industrial sector. She coauthored more than 80 papers in international journals and conferences and ten patents on RFID sensing systems. She is also listed in the PLOS 2023 ranking of the Top 2% Scientists Worldwide. Her research interests include wireless health monitoring through wearable and implantable radio frequency/mm-wave identification techniques and pervasive sensing paradigms for the food sector and Industry 4.0.

Luca Catarinucci (Senior Member, IEEE) is an Associate Professor of electromagnetic fields with the Department of Innovation Engineering, University of Salento, Italy, and holds the Chair of "Microwaves" and "Electromagnetic Solutions for Hi-Tech," and leads a dynamic Research Group with a keen focus on RFID and cutting-edge electromagnetic technologies in the realm of IoT. His collaborations extend to numerous research teams, delving into areas such as antenna arrays, the manufacturing of antennas, and the role of 3-D printing in electromagnetics, among others. He authored over 200 papers in international journals and conferences, and four chapters in internationally recognized books. He is also the co-inventor of two National patents. His research interests include the deployment of advanced electromagnetic simulation tools, the electromagnetic characterization of diverse materials, and the application of time-domain reflectometry for the qualitative and quantitative assessment of fluids. A significant part of his current research interests include deeply rooted in RFID-related pursuits, spanning across a broad spectrum including antenna and system design, the seamless integration of sensors and RFID tags, innovative strategies for RFID-based robot navigation, and pioneering methods for tag characterization, optimization, and design.

Prof. Catarinucci is the Chair of the IEEE Technical Committee on Additively Manufactured Electronic Systems and a Vice President of Technical Activities at the IEEE Council on RFID (CRFID) from 2022 to 2023. As of now, he is the President-Elect of the IEEE Council on RFID for the two-year term from 2024 to 2025.

Riccardo Colella (Senior Member, IEEE) received the M.Sc. degree (Hons.) in telecommunication engineering and the Ph.D. degree from the University of Salento, Lecce, Italy, in 2010 and 2015, respectively.

He is currently a Researcher of electromagnetic fields area with the Department of Innovation Engineering, University of Salento. He has authored about 150 papers that appeared in international journals and at national and international conferences, two book chapters with international diffusion, and a patent. His research interests include the design of innovative RFID antennas, wirelessly powered IoT sensing systems, antennas for healthcare applications, and novel RF electronic devices and antennas in 3-D printing technology.

Giorgio Montisci (Senior Member, IEEE) received the M.S. degree in electronic engineering and the Ph.D. degree in electronic engineering and computer science from the University of Cagliari, Cagliari, Italy, in 1997 and 2000, respectively.

Since February 2022, he has been a Full Professor of electromagnetic fields at the University of Cagliari, teaching courses in electromagnetics and microwave engineering. He has authored or coauthored more than 80 articles in international journals. His current research interests include the analysis and design of waveguide slot arrays, RFID antennas, wearable antennas, numerical methods in electromagnetics, and microwave circuits and systems.

Prof. Montisci was awarded IEEE ACCESS Outstanding Associate Editor of 2020 and 2021. He is an Associate Editor of IEEE ACCESS, *IET Microwaves, Antennas and Propagation*, and *IET Electronics Letters*, and an Academic Editor of the *International Journal of Antennas and Propagation*.

Gaetano Marrocco (Senior Member, IEEE) received the M.S. degree in electronic engineering and the Ph.D. degree in applied electromagnetics from the University of L'Aquila, Italy, in 1994 and 1998, respectively.

He was a Researcher at the University of Rome "Tor Vergata," Rome, Italy, from 1994 to 2014, where he was an Associate Professor of electromagnetics from 2013 to 2017, has been a Full Professor since 2018, and currently serves as the Director of the Medical Engineering School. He is the Director of the Pervasive Electromagnetics Laboratory (www.pervasive.ing.uniroma2.it) and the Co-Founder and the President of the University spin-off RADIO6ENSE (www.radio6ense.com), which is active in the short-range electromagnetic sensing for the Industrial Internet of Things, smart manufacturing, automotive and medical device. The first phase of his career was devoted to the research on time-domain electromagnetics with application to structural, broadband, and ultrawideband antennas for Satellite (ESA, ASI), avionic, and naval (Leonardo) communications. Then, since 2002, he has been investigating sensor-oriented miniaturized antennas for Biomedical engineering and radio frequency identification (RFID), contributing to the move from the RF labeling of objects to the passive sensor networks in the Internet of Things era. He carried out pioneering research on body-centric battery-less wireless sensors concerning textile RFID antennas, tattoo-like sensors (flexible and stretchable epidermal electronics), laser-induced-graphene wireless devices, and radio-sensors embedded inside implanted prostheses. He is listed in the PLOS ranking of the Top 2% Scientists Worldwide (source: University of Stanford).

Prof. Marrocco was formerly an Associate Editor of IEEE ANTENNAS AND WIRELESS PROPAGATION LETTERS and IEEE JOURNAL OF RADIO FREQUENCY IDENTIFICATION. Currently, he is a Track Editor for IEEE JOURNAL OF FLEXIBLE ELECTRONICS and the Chair of the Italian delegation URSI Commission D Electronics and Photonics.

Open Access funding provided by 'Università degli Studi di Cagliari' within the CRUI CARE Agreement